

See discussions, stats, and author profiles for this publication at: <https://www.researchgate.net/publication/375552534>

# Automatic Control System for Precise Intravenous Therapy Using Computer Vision Based on Deep Learning

Article in IEEE Access · November 2023

DOI: 10.1109/ACCESS.2023.3328568.

CITATIONS

0

READS

30

4 authors, including:



Jaehwang Seol

Gachon University

7 PUBLICATIONS 7 CITATIONS

[SEE PROFILE](#)



Kwanggi Kim

National Cancer Center Korea

347 PUBLICATIONS 9,241 CITATIONS

[SEE PROFILE](#)

## RESEARCH ARTICLE

# Automatic Control System for Precise Intravenous Therapy Using Computer Vision Based on Deep Learning

JAEHWANG SEOL<sup>1,2</sup>, SANGYUN LEE<sup>2</sup>, JEONGYUN PARK<sup>3</sup>, AND KWANG GI KIM<sup>1,2,4,5</sup><sup>1</sup>Department of Biomedical Engineering, College of Health Science, Gachon University, Incheon 21936, Republic of Korea<sup>2</sup>Medical Devices R&D Center, Gachon University Gil Medical Center, Incheon 21565, Republic of Korea<sup>3</sup>Department of Clinical Nursing, University of Ulsan, Seoul 05505, Republic of Korea<sup>4</sup>Department of Biomedical Engineering, College of Medicine, Gachon University, Incheon 21565, Republic of Korea<sup>5</sup>Department of Health Sciences and Technology, Gachon Advanced Institute for Health Sciences and Technology (GAIHST), Gachon University, Incheon 21999, Republic of Korea

Corresponding author: Kwang Gi Kim (kimkg@gachon.ac.kr)

This work was supported by the Gachon Gil Medical Center under Grant FRD2022-12-02.

**ABSTRACT** Intravenous (IV) therapy provides a rapid therapeutic effect. However, errors in infusion rate can lead to over-dosing and under-dosing, potentially causing severe side effects for patients. To prevent incidents, medical staff visually monitors medication injection information (*MIF*) such as current flow rates (*CFR*) and injection volume. In this study, we propose an internet of things (IoT) system that automatically controls the *CFR* and remotely monitors the *MIF*. First, a peristaltic pump is designed to infuse parenteral fluids based on the “drop-by-drop” phenomenon. Second, a computer vision-based on deep learning algorithm provides real-time video and counts the fluid dropping to derive the *MIF*. Finally, the *CFR* is automatically applied as a feedback signal to regulate the infusion cycle of the peristaltic pump. After embedding all systems in our prototype, we evaluate the system performance according to IV therapy protocols used in clinical practice. In our experiments, the mean accuracy of the fluid injection using the peristaltic pump was 99.23% and the dropping count was the highest at 98.25%. Furthermore, the average accuracy of the *CFR* using the feedback system was 99.3%. Based on our results, we confirmed that automated control of infusion rate is possible in IV therapy and computer vision-based on deep learning can be utilized for feedback sensors and monitoring system. Therefore, we believe that our method is the practical solution that can increase patient safety and work efficiency of clinical staffs.

**INDEX TERMS** Intravenous therapy, infusion flow rate, feedback control, computer vision-based on deep learning, Internet of Things, vision monitoring.

## I. INTRODUCTION

Intravenous (IV) therapy is a traditional treatment that has been used in emergency rooms, operating rooms, and intensive care units (ICUs) for over a century [1], [2], [3]. In particular, IV therapy provides rapid therapeutic effects by invasively infusing drugs (e.g., parenteral fluids, electrolytes, and nutrients) that cannot be injected through the subcutaneous tissue and oral cavity of patients [4], [5].

An intravenous set (IVS), which is commonly used for IV therapy, consists of an IV bag containing the fluid, IV tube

The associate editor coordinating the review of this manuscript and approving it for publication was Santosh Kumar<sup>1</sup>.

and needle to deliver fluid into a vein, and drip chamber detecting the “drop-by-drop” phenomenon. Additionally, a roller clamp controls the infusion rate of the fluid; however, it has low precision owing to its manual operation and high regulation sensitivity [6]. Therefore, several techniques have been proposed for precise control.

The first technique is an IV flow regulator, a single-use manual valve that uses gravity to control injection. It allows more precise control over the flow rate than the roller clamp, but an error is observed between the targeted and actual flow rates depending on the viscosity of the solution [7], [8]. The second technique involves an infusion pump, an electronic device that controls the flow rate more precisely than manual

units. In addition, numerical information regarding fluid injection can be customized and monitored by medical staff. However, errors are still observed in clinical practice today [9], [10]. For example, medical staffs may be confused when entering analog-calculated injection information into the infusion pump. In particular, the incorrect conversion of units (e.g., hour and minute, weight and volume) and misapplication of decimal points and flow rates have been identified as systemic causes of errors [11]. Finally, syringe pumps have been used to intravenously administer small amounts of fluid for critical care or anesthesia. The plunger of the syringe is pushed at a constant pressure to control the injection volume, and the fluid velocity sensor measures the flow rate. When the targeted flow rates are low, delayed operation times, delayed opening and closing notifications, and irregular flow rates are consistently recognized as functional improvements [12], [13].

In addition to the previous techniques, various studies based on digitalization have been conducted [14], [15], [16], [17]. The study in [6] proposed an Internet of Things (IoT) system for monitoring and controlling injection volume. The fluid volume in the IV bag was measured using a liquid level sensor and the type of drug was detected using a color image sensor; simultaneously, the roller clamp remotely controlled the flow rate based on commands from the web browser. Some of the material of the IV bag consist of polyvinyl chloride (PVC); this means that the shape can be changed, which can lead to measurement errors owing to different fluid levels even if the fluid volume in the IV bag remains the same. In addition, the roller clamp non-linearly controls the flow rate, resulting in low precision. Meanwhile, the study in [18] also proposed the use of an IoT system for measuring and regulating the infusion volume. The light-emitting diode (LED) laser and photodiode detected the fluid dropping to compute the injection volume. The infusion flow rate was then induced to have a linear relationship with the range in which the roller clamp compresses the IV tube. The LED laser has a low divergence angle, and the drops are very small. These conditions may necessitate the accurate focusing of the drops, as they may easily be missed because of their own wobbling and tilting of the drip chamber.

In addition to IoT, artificial intelligence (AI) has been utilized in studies. In [19], the most appropriate computer vision-based on model to detect the liquid level in the IV bag was determined. The performances of you only look once (YOLO)-v3, region-based convolutional neural network (RCNN), Fast-RCNN, and speeded-up robust feature (SURF) were compared on a single image, and YOLO-v3 exhibited the highest precision, recall, and intersection over union (IOU) results. These findings may suggest that additional studies are required to evaluate detection performance in a real-time environment, as well as single frame. Another AI study in [20] and [21] used a camera and a computer vision-based on deep learning model to obtain the injection volume and flow rate in real-time. In the drip chamber, drops were generated and categorized into the initial and final stages.

Subsequently, the number of dropping and flow rates were calculated during the alternation of the stages. Since this study focused on remote monitoring detection, the additional ability to control infusion rate is expected to be synergistic with medical staff.

Despite efforts to provide precise IV therapy, IV errors cause serious side effects than other therapies [22], [23]. In particular, there are four types of clinical errors (e.g., wrong flow rate, wrong volume, wrong mixture, and drug incompatibility), and the potential severity is categorized into minor (levels 1–2) and serious (levels 3–5). According to the literature, the proportion of cases with at least one clinical error among all errors was 63.9% (363/568; 95% CI, 60.0% to 67.9%), of which 27.3% were serious errors. Among the 363 errors, the percentage of wrong flow rates was 73.3%, of which 35.7% were serious [24]. In another analysis, errors in the administration procedure during the entire process of IV therapy were 32.1% (1104/3433; 95% CI, 30.6% to 33.7%); among them, the wrong flow rate was the most prevalent at 57.9% (536/925; 95% CI, 54.7% to 61.1%) [25]. With regard to flow rate, low infusion rates can cause dehydration, circulatory shock, while high infusion rates can result in an imbalance between electrolytes and fluids [5].

In conclusion, an incorrect flow rate is the most frequent error and can cause severe damage to patients. Therefore, studies should be conducted that combine medical expertise with advanced technology to prevent these harmful effects [26], [27], [28]. In this study, we propose an IoT system that automatically controls the flow rate and remotely monitors the drip chamber to enable precise IV administration. The overall method is summarized as follows.

- We built an IoT foundation for data communication, remote monitoring, and feedback control.
- We designed a peristaltic pump for fluid infusion.
- We applied the computer vision-based on deep learning algorithm to detect “drops” and count the “dropping” in the drip chamber.
- We designed the acceleration and deceleration profiles of the motor to optimize the dropping count system.
- We designed a feedback control system for automated flow regulation by integrating the aforementioned steps.

The proposed system is expected to allow medical staff to monitor drug infusions and quickly recognize emergencies without walking around the ward.

## II. DESIGN METHOD

### A. PROTOTYPE AND IOT FOUNDATIONAL DESIGN

Fig. 1 illustrates the fabricated prototype device with a mounted drip chamber and sequence of the drop-by-drop phenomenon. In particular, the specific meaning of each term is defined to avoid confusion with synonyms used in clinical practice with reference to the Fig. 1.

1. Total volume (mL) - volume of parenteral fluids in the IV bag.
2. Injection volume (mL) - volume of parenteral fluids infused into the patient.

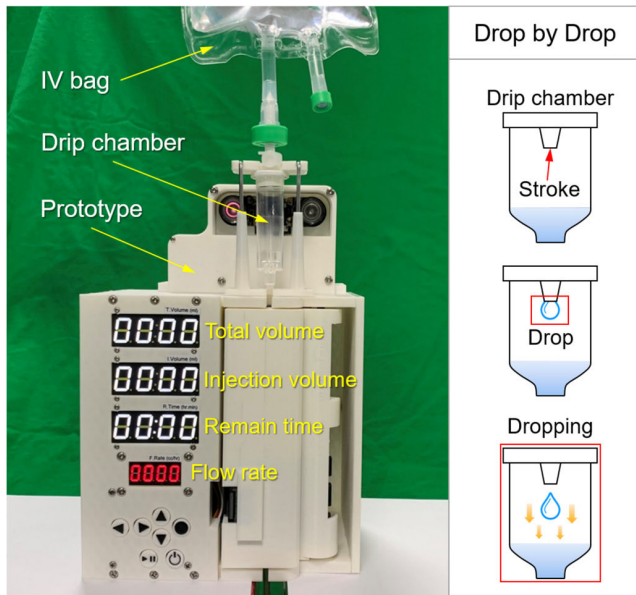


FIGURE 1. Fabricated prototype and sequence of the drop-by-drop phenomenon.

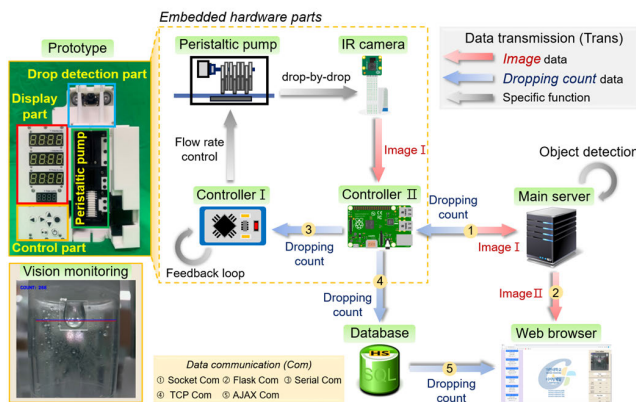


FIGURE 2. IoT communication process for data transmission, feedback flow rate control, and vision monitoring of the drip chamber in real-time environment.

3. Remain time (hour/min) - time remaining until the infusion is completed.
4. Flow rate (cc/hr) - injection volume per remain time.
5. Drop - trickle shape of fluids generated by the stroke.
6. Dropping - drop falling out of the stroke.
7. One rotation - 360° rotation of the motor.
8. Frame - output image through object detection model.

Fig. 2 shows the IoT communication (Com) process used for automated flow rate control and web browser monitoring. Before communication begins, power is applied into the hardware modules and the button located on the bottom-left is pressed to activate all modules for the first time. The prototype then operates in four stages. The control part customizes appropriate numerical value of the medication injection information (*MIF*) which consists of the total volume, injection volume, remain time, and flow rate. In the display part, each 4-segment LED (ADA-878) numerically

indicates the value of the *MIF*. The peristaltic pump periodically squeezes the IV tube to infuse the parenteral fluids into the patient, and the drop detection part films the drip chamber to detect “drop” and “dropping” in real-time.

1) IMAGE DATA TRANSMISSION

After fluids are infused based on the drop-by-drop method, image I (drip chamber) is captured by the infra-red (IR) camera (YR-030), stored in controller II (Raspberry Pi 4B), and transmitted to the main server, sequentially. Image I is then used as the input data for the object detection model to detect drop and dropping. After detection by the model, image II (output data) is transmitted to the web browser as a single frame source that makes up the live video.

2) DROPPING COUNT TRANSMISSION

When the detection model outputs Image II, dropping can also be counted. In particular, the dropping count data are only transmitted to controller II when the count increases. The received data are then immediately conveyed to the database (DB) and controller I (SZH-EK034). The DB stores incoming data in the time domain and transmits them to the backend server in the web browser. Finally, the *MIF* is updated and displayed as a number in the web browser. Controller I also receives the dropping count data and computes the current flow rate (*CFR*) using the *MIF* as a basis. The peristaltic pump is then controlled via a feedback signal which generated as a result of the difference between the target flow rate and the *CFR* computed by Controller I.

3) DATA COMMUNICATION

Controllers I and II are embedded in the prototype and have serial communication at a 115,200 baud rate for rapid sharing of the dropping count. Controller II and main server are connected via socket Com to share Image I and dropping count in both directions. Flask Com is used for transmitting image I to the web browser. TCP Com is used to connect controller II and DB, and AJAX Com helps transmit the DB data to the web browser. All connections are configured with wireless Com except for the serial Com.

B. DESIGN OF THE INFUSION PUMP

1) DESIGN OF THE PERISTALTIC PUMP

A peristaltic pump is designed to squeeze the IV tube based on the drop-by-drop phenomenon as shown in Fig. 3. In particular, a side view of the fabricated hardware and mechanical parts is schematized. The cams mounted on the shaft are rotated by a step motor and push the followers to press on the IV tube. Twelve cams and followers are used. Camrids I and II are designed on the opposite side of the followers from the IV tube. Camrid I is a flat plate that covers 12 followers, while camrid II is fixed by a locker to maintain its position. The compression spring is located between camrids I and II. Therefore, when the followers press on the IV tube, an elastic force corresponding to the reaction

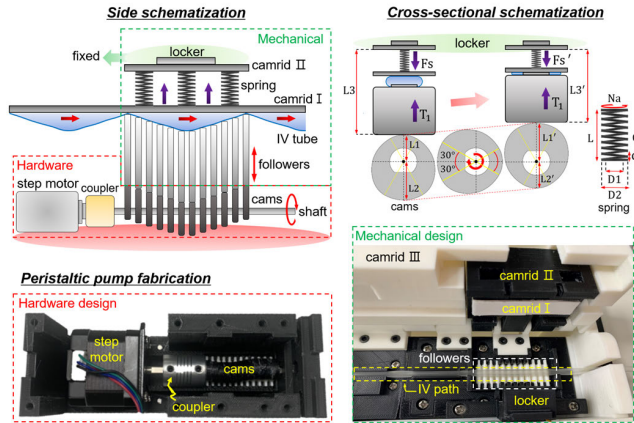


**FIGURE 3.** Design of the peristaltic pump for IV tube squeezing based on the drop-by-drop method. The force and motion mechanisms are analyzed with side and cross-sectional schematizations of the fabricated peristaltic pump.

force also pushes camrid I. Consequently, the IV tube is compressed on both sides.

## 2) ANALYSIS OF THE FORCE AND MOTION MECHANISM

The side and cross-section are schematized to analyze the force and motion mechanism of the peristaltic pump. All 12 cams have the same radius (mm) from the rotational axis. Therefore, sum of the shortest ( $L1, L2'$ ) and longest ( $L1', L2$ ) radii is always equal, as expressed in Eq. (1).

$$L1 + L1' = L2 + L2', (L1 = L2' \text{ and } L1' = L2) \quad (1)$$

Additionally, the length from the shaft axis to camrid II is always constant as shown in Eq. (2). The cam is not perfectly circular, but has a partially protruding radius. Therefore, the radius at which the cam faces the follower is between  $L1$  and  $L1'$ , and the pressure intensity in the IV tube depends on the angle of rotation. For example, the IV tube is opened if the radius is  $L1$ , whereas the tube is closed if the radius is  $L1'$ .

$$L1 + L3 = L1' + L3' \quad (2)$$

All cams have the same outline shape and are symmetrical based on the centerline that passes through the  $L1$  and  $L2$  radii. In addition, the lengths of  $L1$  and  $L2$  are kept the same by a range of  $\pm 30^\circ$  from the centerline and the  $N$ -th cam has a shaft hole with a phase shift of  $30^\circ \times N, (N=1 \text{ to } 12)$ . Therefore, the 12 cams sequentially have  $L1'$  in one rotation of the motor, and then the facing followers repeatedly open and close the IV tube to induce unidirectional flow.

The modulus of elasticity  $K$  is an intrinsic characteristic of springs. The load  $P$  applied to the spring is defined by the length of the deflection  $\delta(mm)$  and  $K$ , as expressed by Eq. (3).  $P$  can also be converted to an elastic force  $F_s$  by multiplying with the gravitational acceleration ( $a=9.81m/s^2$ ), as in Eq. (4).

$$P(kgf) = K \times \delta \quad (3)$$

$$F_s(N) = P \times a \quad (4)$$

**TABLE 1.** Summary of the spring properties.

Symbol	Meaning of symbols	Magnitude
$G$	modulus of transverse elasticity	7500 kg/mm <sup>2</sup>
$d$	wire diameter of coil	1.2 mm
$D1$	coil inner diameter	8.6 mm
$D2$	coil outer diameter	11 mm
$Na$	number of effective turns	3.2
$L$	free height (length)	7 mm

The characteristic parameters of the spring are defined during manufacture, as summarized in Table 1, and  $K$  can be calculated using Eq. (5).

$$K(kg/mm) = \frac{G \times d^4}{8 \times Na \times D^3} \quad (5)$$

$G$  indicates the standard value of the transverse elasticity modulus of the stainless steel material, while  $d$  represents the wire diameter of the coil.  $D$  is obtained by calculating the average inner and outer diameters of the spring.  $Na$  is the number of effective turns in the spring and  $L$  is the length of the free field without any load. Therefore,  $K$  is estimated as 0.645 kg/mm and  $F_s$  can be also calculated if length of the deflection ( $\delta$ ) is known.

Meanwhile, we use a vernier caliper (M500-153M) and force meter (DS2-100N) to measure the closing conditions of the IV tube, and observe that a force greater than 4 N should be applied over a depth of 1.7 mm. Therefore,  $L1$  is designed to be 4 mm so that the followers can press on the IV tube by 0.5 mm ( $\delta = 0.5mm$ ); thus  $F_s$  approximates 0 N and the IV tube opens. In addition,  $L1'$  is designed to be 6.7 mm so that  $\delta$  can be 1 mm; thus  $F_s'$  approximates 6.28 N and the IV tube closes.

Three compression springs are used, each located in the center of the one-third of the camrid I area. If we assume that a follower vertically presses a single spring with no force distribution,  $F_s' = 6.28$  N. Therefore, we determine that the regulated motor torque  $T_1$  should be four times higher than  $F_s'$  at  $\delta = 1$ , as expressed in Eq. (6).

$$T_1(N \cdot m) \geq 4 \times F_s', (\delta = 1) \quad (6)$$

All the parts of the peristaltic pump are printed using a 3D printer (Raise-3D Pro2, Raise3D). The internal strength of the PLA filament is set to 100% to prevent breakage and deformation of the parts. The surfaces of the cams are lubricated to minimize friction between cams and followers.

## C. DROP DETECTION AND DROPPING COUNT

When the peristaltic pump is running, fluid dropping can occur. In order to detect these dropping, we investigate prior study to select an appropriate object detection model. As a one-stage detector, the YOLO-v1 shows a high detection speed up to 45 FPS than previously proposed models. In addition, the model network simultaneously predicts a single bounding box and class probability. However, it has a lower accuracy with 63.4 mean average precision (mAP)

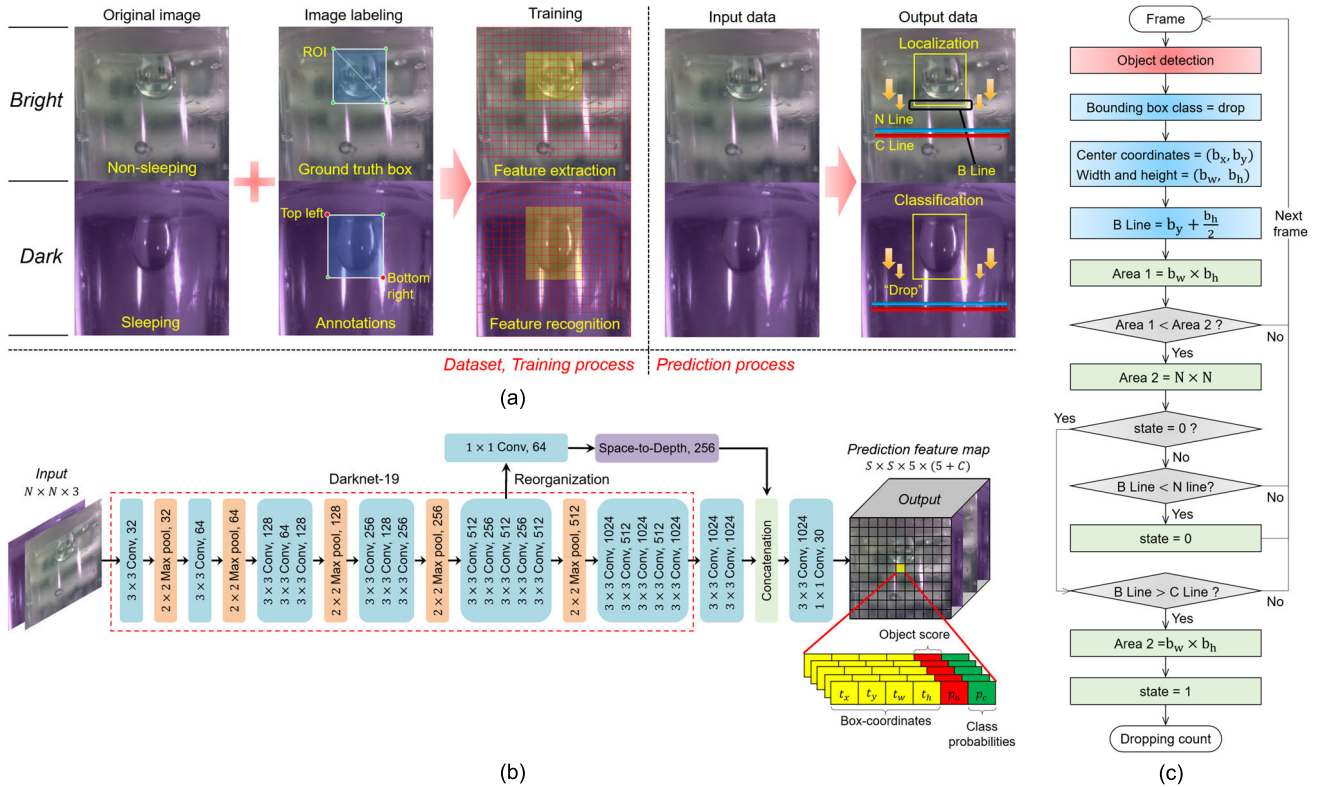


**FIGURE 4.** Process of drop detection and dropping count in bright and dark environments. (a) Dataset, training, and prediction procedure for drop detection. (b) Drop detection procedure using YOLO-v2 architecture. (c) Dropping count flowchart using the line passing algorithm.

compared to other models due to the challenge of predicting small objects with ambiguous boundaries [29].

The YOLO-v2 modified backbone network as darknet-19 to improve the classification performance while maintaining the FPS quality. In addition, the model network uses various methods such as k-means clustering and anchor box, increasing classification and localization performance up to 78.6 mAP. Therefore, we applied the YOLO-v2 model because it can quickly provide the coordinates of the bounding box with high accuracy when drop detection is required in a real-time IoT environments [30].

### 1) DATASET, TRAINING AND PREDICTION PROCESS

The entire process of drop detection and dropping count is shown in Fig. 4, and NVIDIA Geforce RTX 2030 Ti is used as the graphics processing unit (GPU) in this study. Fig. 4(a) shows the overall procedures about drop detection. To create datasets, the original images are collected by capturing the drip chamber using the IR camera. In particular, 800 bright and 800 dark sight images are obtained, considering the non-sleeping and sleeping environments in the ward, respectively. Then, the ground truth (GT) box is created in the region of interest (ROI) using a *labelimage* program. Therefore, the coordinates at the top left and bottom right of the GT box are annotated in the training data format (.xml). After establishing the datasets, the YOLO-v2 model is trained by simultaneously inputting the original images and

annotation data and optimizing the gradient. During training, the model extracts and recognizes the features of a drop in an image. Subsequently, the prediction model performs drop classification and localization, providing the coordinate information to the dropping count method.

### 2) DROP DETECTION PROCEDURE

Fig. 4(b) shows the architecture of the YOLO-v2 model used for drop detection. All input images contain red, green, and blue channels. The feature map is reorganized into four layers by passing through the 17th layer and  $1 \times 1$  convolutional (Conv) layer and concatenated with the 25th layer to increase the detection performance of small and large drops. After creating the datasets, we performed k-means clustering ( $k=5$ ) to pre-determine the five optimal anchor boxes that most closely match the GT boxes per one grid cell. The training model then simplifies the task of prediction, makes learning easier, and increases recall for drops. A well-trained model can predict five anchor boxes in the each  $S \times S$  grid cells, and each anchor box can estimate four coordinates  $(t_x, t_y, t_w, t_h)$ , an object score  $p_o$ , and a class probability  $p_c$ . As we aim to detect a single drop in a  $544 \times 544$  image,  $S$  is 17 and drop is classified and localized based on the 6 vectors, consequently.

By multi-scale training, trained model can provide robust detection performance and allow us to freely choose the input size of the image based on the trade-off feature between FPS and mAP. We used a  $544 \times 544$  high-resolution image as input

data because the output image will be sent to the web server and the frames should be of high quality when displayed as a video in the web browser. Finally, in order to maintain high precision overall drop size, the IR camera and drip chamber were manually positioned through 3D design so that the drops were centered in the image.

### 3) DROPPING COUNT PROCEDURE

Fig. 4(c) shows an algorithm flowchart of the dropping count in a real-time environment. A single image that passes through the prediction model becomes a single frame. In addition, the top-left corner of the frame is designated as the base point and the bounding box of the drop is created in the frame. The central coordinates of the bounding box are represented by  $(b_x, b_y)$  while  $b_w$  and  $b_h$  indicate the width and height, respectively. Therefore, the y-axis value of the bottom line (*B Line*) is calculated by Eq. (7).

$$B\ Line = b_y + \frac{b_h}{2} \quad (7)$$

Immediately after drop detection, *Area 1* is calculated by conduct of  $b_w$  and  $b_h$ . When *B Line* passed through the count line (*C Line*) *Area 2* also computed by multiplying  $b_w$  and  $b_h$ , counting one dropping. Therefore, if dropping occurs and a new small drop is generated, *Area 1* is smaller than *Area 2* and then value of *Area 2* is initialized to  $N \times N$  which is equal to the entire frame area, as given by Eq. (8).

$$Area\ 2 = N \times N, (Area\ 1 < Area2) \quad (8)$$

Dropping is counted when *B Line* passes through *C Line*. However, if no dropping occurs in one rotation of the peristaltic pump and it simply hangs on the stroke, *B Line* may hover around *C Line*. Therefore, the vibration of the *B Line* may cause an accumulation of dropping counts in consecutive frames. This problem is resolved by inserting a noise line (*N Line*) into the image, and the conditions are added as shown in Eq. (9).

$$state = 0, (B\ Line < Nline) \quad (9)$$

The *state* variable only becomes 0 on a frame when *B Line* passes through *N Line*, and becomes 1 again when *B Line* passes through *C Line*.

### D. OPTIMIZATION OF THE DROPPING COUNT

As shown in Fig. 2, the controller II and peripheral devices share data when the dropping is counted. However, a time delay occasionally occurs when a single thread of controller II simultaneously handles the serial, socket, and TCP Coms. When consecutive dropping occurs during the time delay, the second dropping is may not considered because Eqs. (8) and (9) are not satisfied. To resolve this problem, we apply acceleration and deceleration (*A/D*) control to the motor that operates the peristaltic pump. Fig. 5 shows the application method of *A/D* control and simulation results as a graph.

The step motor is driven by a pulse signal received from the motor driver (DRV 8834). The initial micro-step of the driver

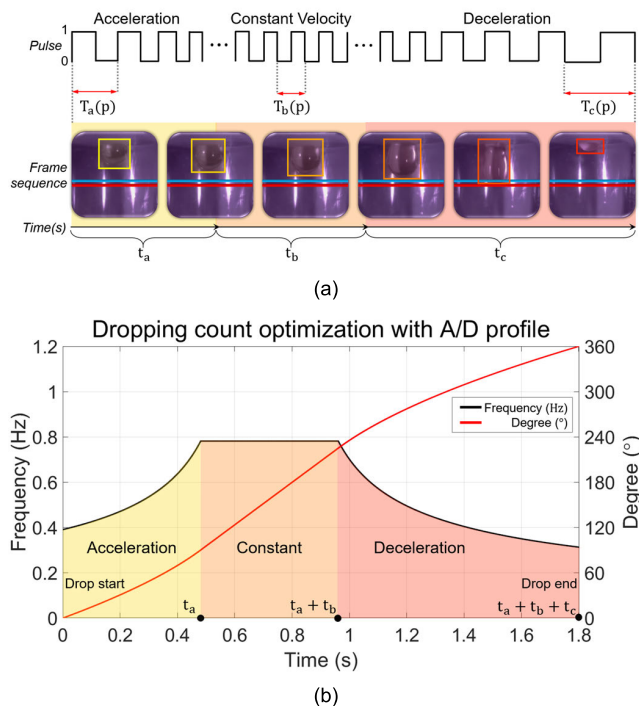


FIGURE 5. *A/D* control for dropping count optimization. (a) *A/D* control using pulse period modulation within each velocity profile. (b) Plot of the motor frequency and degree variation in the time domain.

is  $1.8^\circ$  rotation per pulse, the resolution is then increased by eight times for smooth start and stop impacts with low vibration and noise. Therefore, 1600 pulses are applied for each rotation of the motor. Fig. 5(a) shows the derivation procedure of *A/D* control during one rotation. First, the pulse range is divided into acceleration, constant velocity, and deceleration profiles, which become the conditions in Eq. (10). The duration of each profile is then calculated as  $t_a$ ,  $t_b$ , and  $t_c$  by integrating the pulse periods  $T_n(p)_{(n=a,b,c)}$ . Finally, the total duration of one rotation is given as  $t_{rot}$ .

$$t_{rot}(s) = \begin{cases} \int_0^{P_a} T_a(p) = t_a, (0 \leq p < P_a) \\ \int_{P_a}^{P_b} T_b(p) = t_b, (P_a \leq p < P_b) \\ \int_{P_b}^{P_c} T_c(p) = t_c, (P_b \leq p \leq P_c) \end{cases} \quad (10)$$

In the IV therapy methodology, the symbol Gtt represents the drop per minute (min), and the drop factor is defined as the drop per mL. Therefore, the flow rate (cc/hr) can be calculated as three times the Gtt (drop/min) if the drop factor (drop/mL) is 20 [31], [32]. In this study, we prefer the duration of one rotation to be less than 2.0 s to ensure that the flow rate can be selected within 0-90 cc/hr, as expressed by Eq. (11).

$$t_a + t_b + t_c < 2.0 \quad (11)$$

In the dropping count procedure, we use a serial monitor and experimentally observe that *B Line* passes through *C Line* on

more than half of one rotation. Therefore, we divide the pulse ratios  $P_a$ ,  $P_b$ , and  $P_c$  as shown in Eq. (12), to minimize the y-axis variation of *B Line* per frame. Consequently, *B Line* passes through *C Line* when the constant velocity profile is converted into the deceleration profile.

$$P_a : P_b : P_c = 1 : 1.5 : 1.5 \quad (12)$$

The functions  $T_a(p)$ ,  $T_b(p)$ , and  $T_c(p)$  are derived as shown in Eqs. (13), (14), and (15) based on the preconditions in Eq. (11) and (12). By substituting Eqs. (12)-(15) into Eq. (10), the durations of  $t_a$ ,  $t_b$ , and  $t_c$  are calculated as 0.481, 0.481, and 0.841 s, respectively, which yields  $t_{rot}$  as 1.803 s.

$$T_a(p) = \frac{2(800 - p)}{10^6}, (0 < p < 400) \quad (13)$$

$$T_b(p) = \frac{800}{10^6}, (400 < p < 1000) \quad (14)$$

$$T_c(p) = \frac{2(p - 600)}{10^6}, (1000 < p < 1600) \quad (15)$$

The angular velocity  $\omega$  of the motor is the variation in the rotation angle  $\Delta\theta$  for a variation in  $T_n(p)_{(n=a,b,c)}$ , as expressed in Eq. (16). In particular,  $\Delta\theta$  is fixed at  $0.225^\circ$  because micro-step has a resolution of eight times, and angular velocity  $\omega$  is finally translated as a frequency (Hz).

$$\omega(\text{rad/sec}) = \begin{cases} \frac{\Delta\theta}{T_a(p)}, (0 < p < 400) \\ \frac{\Delta\theta}{T_b(p)}, (400 < p < 1000) \\ \frac{\Delta\theta}{T_c(p)}, (1000 < p < 1600) \end{cases} \quad (16)$$

Fig. 5(b) shows a plot of the *A/D* profile simulation. The black and red lines represent the frequency and rotation angle in the time domain, respectively. An analysis of the graph shows that half of one rotation is completed at 0.8 s and the constant velocity profile enters the deceleration profile within 0.2 s. Therefore, the y-axis variation of *B Line* per frame is decreased in the deceleration profile, avoiding loss of dropping from time delay.

### E. DESIGN OF THE FEEDBACK CONTROL SYSTEM

Errors in volume can occur because the peristaltic pump do not always control one drop (0.05 mL) per rotation exactly. Therefore, we propose an automatic flow rate control system that transmits feedback signals derived from the *MIF*. Fig. 6 shows the procedure to derive and apply the feedback control using a flowchart of the entire system.

#### 1) PROTOTYPE AND PERISTALTIC PUMP

After the prototype is powered on, IV tube is inserted into the IV path. The signal from the force sensor (F015WNGX, Honeywell) is amplified using an operational amplifier (INA126, Texas Instruments) to confirm the occlusion of camrids I, II, and III. After camrids are closed, the total volume, injection volume, and remain time are customized

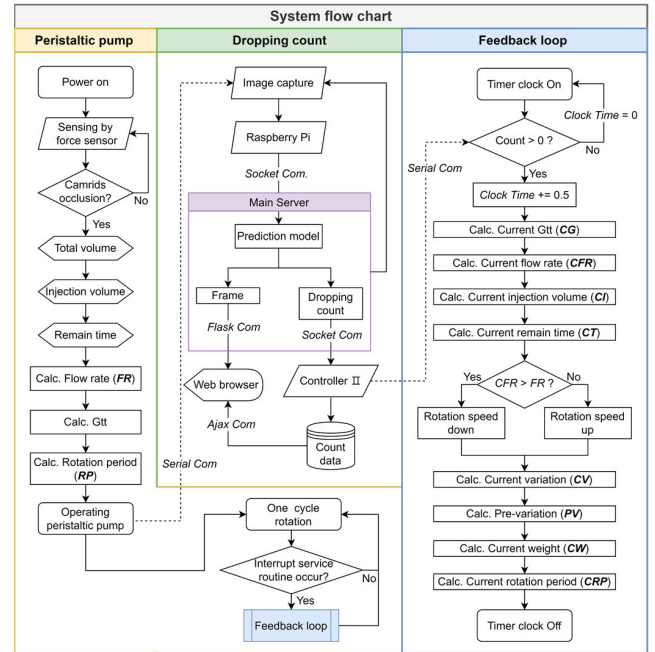


FIGURE 6. Flowchart of the entire system applying the feedback loop algorithm. (\*Calc. indicates calculate).

sequentially. Finally, the targeted flow rate (*FR*) is calculated using Eq. (17) [31], [32].

$$FR(\text{cc/hr}) = \frac{\text{Injection Volume (mL)}}{\text{Remain Time (min)}} \quad (17)$$

We use an IV flow control line (IVS, Insung Medical) with a drop factor of 20 drops/mL. Subsequently, *FR* is converted to *Gtt*, and its reciprocal is used to match one rotation with one dropping. Consequently, the rotation period (*RP*) of the motor, which is recorded in milliseconds (*ms*) with high precision, was simplified as shown in Eq. (18).

$$RP(\text{ms}) = (60 \div Gtt) \times 1000 \quad (18)$$

#### 2) DROPPING COUNT

After calculating the *RP*, the fluid injection is started and frames are extracted by the prediction model. Consecutive frames are transmitted to a web browser for video monitoring, while controller II transmits the counted data to controller I and DB when the dropping is counted. DB transmits the data to a web browser for numerical *MIF* monitoring.

#### 3) FEEDBACK LOOP

After determining *RP*, controller I drives rotation of the peristaltic pump and simultaneously enters the feedback loop designated by an interrupt service routine. In particular, the controller I enters the feedback loop every 0.5 s by setting a timer clock, and the dropping count increases from 0 to 1, the *Clock Time* variable starts accumulating 0.5. Therefore, the current *gtt* (*CG*) is derived from the dropping count and *Clock Time* variable as shown in Eq. (19). The *CFR* then can

be calculated as three times the *CG*, as expressed in Eq. (20).

$$CG \text{ (drops/min)} = \frac{\text{Dropping count} \times 60}{\text{Clock Time}} \quad (19)$$

$$CFR \text{ (cc/hr)} = CG \times 3 \quad (20)$$

The current injection volume (*CI*) indicates the remaining infusion volume, as in Eq. (21). The current remain time (*CT*) is then defined until the parenteral fluid is completely infused, as expressed by Eq. (22).

$$CI \text{ (mL)} = \text{Injection volume} - (\text{count} \times 0.05) \quad (21)$$

$$CT \text{ (s)} = (CI \div FR) \times 60 \quad (22)$$

Controller I compares the speeds of *FR* and *CFR* whenever entering the feedback loop. If *CFR* is faster than *FR*, the rotation interval of the peristaltic pump decreases; if it is slower, rotation interval increases. As the principle of these actions, the feedback signal is applied to the *CRP* by measuring the error between the *FR* and *CFR*. The current variation (*CV*) uses an absolute sign to ensure that the difference between the two speeds (*CFR* and *FR*) remains positive, as shown in Eq. (23).

$$CV \text{ (s)} = 60 \div (|FR - CFR| \div 3) \times 1000 \quad (23)$$

To compensate for the longer duration of the speed difference by making the feedback signal faster, we designate *CV* and the pre-variation (*PV*) as parameters of the feedback weight. Subsequently, the previous value of *CV* is transferred into that of *PV* when entering the next feedback loop, as shown in Eq. (24).

$$PV \text{ (s)} = CV \text{ (s} - 0.5) \quad (24)$$

Therefore, if the speed difference persists, the current feedback weight (*CW*) gradually increases. The initial *CW* value is set to 1.0 and the method for calculating *CW* is shown in Eq. (25).

$$CW(s) = \begin{cases} \text{weight} + 0.02, & CV > PV \\ \text{weight} - 0.02, & CV < PV \end{cases} \quad (25)$$

Finally, the current rotation period (*CRP*) is updated by compensating the *FR* with the product of *CW* and *CV*, as shown in equation (26), which becomes the feedback signal to the peristaltic pump that controls the dropping interval.

$$CRP \text{ (s)} = \begin{cases} RP - CW \times CV, & FR > CFR \\ RP + CW \times CV, & FR < CFR \end{cases} \quad (26)$$

### III. EXPERIMENTAL RESULTS

#### A. EVALUATION OF THE PERISTALTIC PUMP

The performance of the peristaltic pump was evaluated by measuring the precision and accuracy of the fluid injection. In one experiment, the motor was rotated 400 times to infuse the parenteral fluids (20 mL) into a beaker. Feedback system was not applied, and fifteen experiments were conducted. For the entire experiment, we measured the injection volume

every time, as shown in Fig. 7(a). We used an electronic scale to measure the weight of the beaker and recorded the total weight of the injected fluid. In particular, we used a 5% dextrose intravenous solution (D5W, JW Pharmaceutical) with a density of 1.0157 g/mL at controlled room temperature [33], [34]. Therefore, the weight of the injected fluid in each beaker was converted into its volume as shown in Eq. (27).

$$\text{Volume} = \text{Weight} \div \text{Density} \quad (27)$$

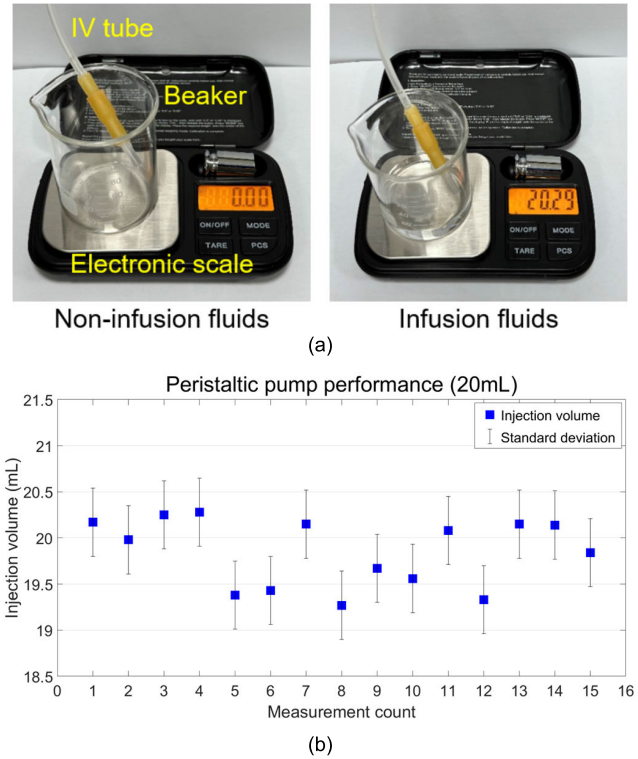


**FIGURE 7. Injection performance evaluation using a peristaltic pump. (a) Measurement of the weight of parenteral fluids using an electronic scale. (b) Results of the injected volume graph from the measurement count.**

Consequently, the measured injection volumes are shown in Fig. 7(b). Based on each volume data, the maximum and minimum volumes were 20.28 mL and 19.27 mL, respectively, while the median volume was 19.98 mL. Additionally, the precision with standard deviation and accuracy of the mean volume to the targeted volume were  $19.85 \pm 0.36$  mL and 99.23%, respectively. Finally, the 95% confidence interval for the mean volume was estimated as 19.64 mL to 20.05 mL.

#### B. EVALUATION OF THE DROPPING COUNT

To evaluate the performance of dropping count system and *A/D* control, we measured the precision and accuracy of the fluid dropping. In particular, we classified the infusion methods into the roller clamp, peristaltic pump (without *A/D*), and peristaltic pump (with *A/D*). Experiments with the *A/D* control were performed twice to increase the amount of

data and the targeted dropping count was set to 200 drops (10 mL). During the measurements, both the prediction model and the experimental environment were identical, and the flow rates were 20, 40, 60, and 80 cc/hr. We controlled the motor using a console in an integrated development environment (IDE) and no feedback system was used. The experimental results for the number of droppings are presented in Fig. 8. The black and red lines represent the roller clamp and constant velocity (without A/D), respectively. The blue and pink lines indicate the 1st and 2nd measurements with A/D control, respectively. Consequently, minimum count is obtained when constant velocity is applied within all flow rate ranges. In contrast, the application of the 1st A/D control resulted in the most dropping at 40 and 80 cc/hr, while the 2nd A/D control resulted in the most dropping at 20 and 60 cc/hr.

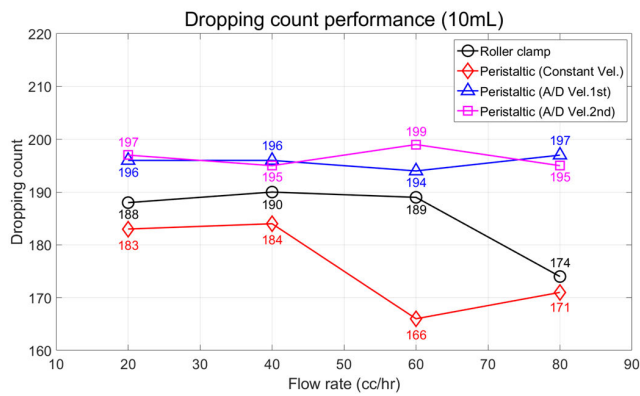


FIGURE 8. Comparative evaluation of dropping count performance using roller clamp, peristaltic pump without A/D control and with A/D control.

TABLE 2. Evaluation of the dropping count performance.

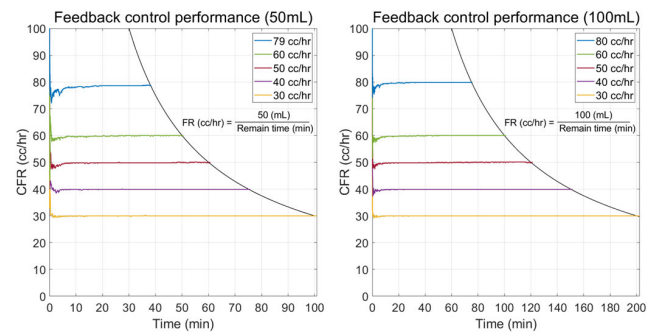
Method	Mean Count	±SD.	%RSD.	%Accuracy
Roller clamp	185.25	6.53	3.53	92.63
Constant Vel.	176.00	7.71	4.38	88.00
A/D Vel. 1st	195.75	<b>1.09</b>	<b>0.56</b>	97.88
A/D Vel. 2nd	<b>196.50</b>	1.66	0.84	<b>98.25</b>

Note: SD., RSD., and Vel. denote the standard deviation, relative standard deviation, and velocity, respectively. The numbers in bold represent the highest dropping count performance.

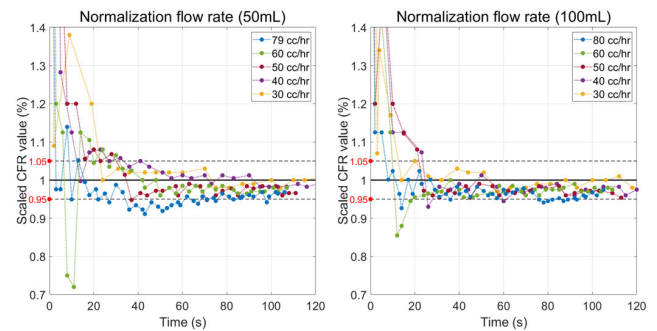
Table 2 presents the experimental results using the evaluation indices. The mean dropping count, which represents the smallest error from the targeted count, was highest for the 2nd A/D control at 98.25%. The precision by standard deviation was highest for the 1st A/D control at (195.75±1.09). In conclusion, the performance of the A/D control was shown to be better than that of the roller clamp and peristaltic pump (without A/D) in all flow rate ranges.

C. EVALUATION OF THE FEEDBACK CONTROL

We designed a feedback loop algorithm based on the foundation of IoT, peristaltic pump, and dropping count system. Finally, we evaluated the performance of the automatic flow rate control using a prototype with an embedded feedback system. We conducted the experiment in a bright sight to match the clinical practice environment. In particular, we set the targeted injection volumes to 50 and 100 mL, which are considered as standard volumes of small-volume parenteral solutions (SVPs) for intermittent IV infusion [35]. In our prototype, we decided the minimum input unit for the remain time is minutes; hence, we set the targeted FR to 30, 40, 50, 60, and 79 cc/hr for the 50 mL injection and set the targeted FR to 80 cc/hr instead of 79 cc/hr for the 100 mL injection. We theoretically calculated a “timer” according to Eq. (17), and the CFR was measured until this “timer” was over. It must be noted that the remain time and “timer” are different words. The initial time setting is identical, but the remain time is updated using the CI and CFR and then converted to CT. In contrast, the “timer” is naturally dwindled by the oscillator inside the controller I.



(a)



(b)

FIGURE 9. CFR performance evaluation using feedback control. (a) Real-time traced CFR dots from the 50 mL and 100 mL injections. (b) Normalized CFR markers distributed around the steady-state.

The measured CFR was extracted from the DB and displayed in the graph as shown in Fig. 9. In the 50 mL and 100 mL injections, feedback control was performed so that the numerous dots that yield the CFR values followed the targeted FR as shown in Fig. 9(a). All CFR produced a linear form without slow or rapid infusion rates and then stopped at the end of the “timer” after completing all injections.

**TABLE 3.** Evaluation of the feedback control performance.

Injection Volume	Targeted Flow rate (cc/hr)	Timer (min)	Feedback Control Evaluation					
			Mean <i>CFR</i>	$\pm$ SD.	%RSD.	%Accuracy	ST.(s)	ET.
50 mL	30	100	<b>29.95</b>	5.38	17.97	<b>99.83</b>	<b>24</b>	<b>4</b>
	40	75	39.88	<b>4.92</b>	12.35	99.70	36	8
	50	60	49.78	5.09	10.23	99.57	37	8
	60	50	59.53	6.02	<b>10.10</b>	99.22	33	11
	79	38	77.49	7.97	10.28	98.09	99	1/12/41
100 mL	30	200	<b>30.00</b>	3.69	12.29	<b>100.00</b>	<b>14</b>	<b>4</b>
	40	150	39.89	3.54	8.88	99.73	65	6
	50	120	49.85	3.73	7.48	99.70	24	6
	60	100	59.87	<b>3.12</b>	<b>5.21</b>	99.78	20	6
	80	75	79.29	5.57	7.02	99.11	93	7/39

Note: *CFR*: current flow rate, *SD*.: standard deviation, *RSD*.: relative standard deviation, *ST*.: settling time to reach steady-state (within 5%), and *ET*.: entering time of the markers. The numbers in **bold** represent the highest performance of the feedback control.

Table 3 lists the evaluation indices of feedback control. In the 50 mL injection, the mean *CFR* indicating the smallest error from the targeted *FR* was 29.95 cc/hr and the accuracy was the highest at 99.83%. The highest value of the precision with standard deviation was 39.88±4.92 cc/hr. For the 100 mL injection, the mean *CFR* indicating the smallest error from the targeted *FR* was 30.0 cc/hr and the accuracy was the highest at 100.0%. The best value of the precision with standard deviation was 59.87±3.12 cc/hr. Consequently, the average *CFR* accuracy indicates 99.3% over the entire flow rate range (20 cc/hr to 80 cc/hr).

After prototype is activated, Fig. 9(b) shows the trace of markers entering an interval within 5% of the steady-state for 2 min. In particular, the marker contains the outcome of the *CFR* value normalized against the targeted *FR* value. At 30 cc/hr, both the marker for 50mL and the marker for 100mL entered the interval within 5% steady-state in only 4th times.

We measured the settling time, which was the first moment when the marker no longer deviated from the 5% steady-state interval. As a result, the fastest and slowest settling times for the 50 mL injection were 24 s and 99 s, respectively, with an average time of 45.8 s. For the 100 mL, the fastest and slowest settling times were 14 s and 93 s, respectively, and the mean time was 43.2 s.

**IV. DISCUSSION**

In this study, we propose a feedback system that automatically and precisely controls infusion flow rate during IV therapy. We also present an IoT system that can rapidly respond to IV errors by vision monitoring. To complete the feedback system, we have designed a peristaltic pump as the core actuator, a dropping count system as the feedback sensor, and IoT technology as the basis for system integration. In our experiments, the 95% confidence interval for the mean volume using the peristaltic pump was 19.64 mL to 20.05 mL. Furthermore, the highest mean accuracy of the dropping

count was 98.25% when *A/D*control was applied to the peristaltic pump. Finally, when infusing 50 mL and 100 mL of parenteral fluids using the prototype with embedded feedback system, the average *CFR* accuracy reached 99.3% over the whole flow rate range (20 cc/hr to 80 cc/hr).

Based on our experiments, we confirmed that the flow rate control is possible and provides precise IV management. In addition, we found that computer vision-based on deep learning model can be a major source of feedback sensor and IoT system with vision monitoring capabilities. Therefore, our proposed system is expected to provide various benefits for IV therapy as mentioned below.

- The collaboration of drip chamber monitoring at nursing stations and cross-checking via ward rotation can help prevent infusion errors.
- Bright and dark vision monitoring provides comfortable environment for patients without medical intervention and allows rapid response to emergencies that occur in a 24-hour period.
- The combination of the feedback signals and peristaltic pump make precise infusions, preventing side effects.
- DB can store and reorder the *MIF* through block chain technology [36], making it convenient for medical staff to manage secure patient information.

Meanwhile, we found a few limitations in our study. First, the embedded hardware in our prototype has the potential to overheat the external temperature. This phenomenon can generate small drops on the wall of the drip chamber, leading to errors in drop detection. Although we did not observe any small drops by replacing the IV sets in every experiment, the optimization of the power consumption may be essential. Therefore, we consider that it is necessary to design temperature sensors and cooling fans inside the prototype to ventilate the heat outside, as well as attach heat sinks and cooling fans to the hardware modules.

Second, we used YOLO-v2 prediction model, considering the technical compatibility and single-object detection. We found that 0.8 s time delay can occur when the frames pass through the prediction model and are transmitted to the web browser. We estimate this delay can be caused by a model computing speed (30 to 33 FPS) and Flask communication speed. In addition, our model still has a trade-off feature between prediction speed and accuracy. Therefore, we plan to conduct follow-up studies to evaluate and improve FPS and detection performance by applying a state-of-the-art prediction models to our dropping system and generating image datasets with various sizes and large numbers.

Finally, while conducting IV therapy, infusion of the air into the vein can lead to an air embolism because of the blockage of blood flow [37]. Therefore, we can consider additional air removal systems, such as air optical sensors and air restriction filters, as well as alarm systems so that medical staff can take appropriate action immediately.

According to the International Council of Nurses (ICN), 90% of their members are concerned about nurse stress owing to heavy workloads [38]. In particular, more than 20% of ICU patients receive IV therapy every day, and more than 30% receive it on the first day of their ICU stay [1]. Another analysis shows that there is a 60–80% probability that IV therapy will be selected as the infusion therapy for hospitalized patients [6], and 17.71% of nursing work includes walking in the ward and visually managing IV administration. In the end, managing personal IVs requires a heavy workload and time commitment from nurses, which can lead to potential errors [39]. Therefore, we believe that our proposed system can create a synergy between safe treatment for patients and reduced workload for nurses.

## V. CONCLUSION

We propose an automated flow rate control system for precise infusion during IV therapy. Our system automatically controls the flow rate of parenteral fluids by embedding a feedback system into our prototype. We conducted experiments using the prototype based on the IV therapy protocol used in clinical practice. Our experimental results confirm that feedback control has the potential to achieve 100% accuracy of the infusion flow rate control. Moreover, technology of the remote IV monitoring may increase the efficiency of the nursing workload. Therefore, we believe that our system method applying AI is state-of-the-art work that can provide a suitable alternative for increasing patient safety and efficiency of nursing work.

## REFERENCES

- [1] S. Finfer, J. Myburgh, and R. Bellomo, "Intravenous fluid therapy in critically ill adults," *Nature Rev. Nephrology*, vol. 14, no. 9, pp. 541–557, Aug. 2018, doi: [10.1038/s41581-018-0044-0](https://doi.org/10.1038/s41581-018-0044-0).
- [2] M. L. N. G. Malbrain, T. Langer, D. Annane, L. Gattinoni, P. Elbers, R. G. Hahn, I. De Laet, A. Minini, A. Wong, C. Ince, D. Muckart, M. Mythen, P. Caironi, and N. Van Regenmortel, "Intravenous fluid therapy in the perioperative and critical care setting: Executive summary of the international fluid academy (IFA)," *Ann. Intensive Care*, vol. 10, no. 1, p. 679, May 2020, doi: [10.1186/s13613-020-00679-3](https://doi.org/10.1186/s13613-020-00679-3).
- [3] A. Porsteinsson, R. Isaacson, S. Knox, M. Sabbagh, and I. Rubino, "Diagnosis of early Alzheimer's disease: Clinical practice in 2021," *J. Prevention Alzheimer's Disease*, vol. 8, pp. 371–386, Jun. 2021, doi: [10.14283/jpad.2021.23](https://doi.org/10.14283/jpad.2021.23).
- [4] I. Usach, R. Martinez, T. Festini, and J.-E. Peris, "Subcutaneous injection of drugs: Literature review of factors influencing pain sensation at the injection site," *Adv. Therapy*, vol. 36, no. 11, pp. 2986–2996, Oct. 2019, doi: [10.1007/s12325-019-01101-6](https://doi.org/10.1007/s12325-019-01101-6).
- [5] P. A. Potter, A. G. Perry, P. A. Stockert, and A. Hall, "Foundations for nursing practice," in *Fundamentals of Nursing*, 10th ed. St. Louis, MO, USA: Elsevier, 2021, pp. 2206–2208.
- [6] D. Oros, M. Penčić, J. Šule, M. Čavič, S. Stankovski, G. Ostojić, and O. Ivanov, "Smart intravenous infusion dosing system," *Appl. Sci.*, vol. 11, no. 2, p. 513, Jan. 2021, doi: [10.3390/app11020513](https://doi.org/10.3390/app11020513).
- [7] A. Cherpin, F. Peyron, N. Desmazes-Dufeu, E. Ragni, B. Lassale, and M. Bues-Charbit, "Concerning one case of rupture of a flow regulator: How patient safety procedures contribute to the correct use of medical devices," *Pharmazie*, vol. 76, no. 12, pp. 618–624, Dec. 2021, doi: [10.1691/ph.2021/1752](https://doi.org/10.1691/ph.2021/1752).
- [8] E. Ko, Y. J. Song, K. Choe, Y. Park, S. Yang, and C. H. Lim, "The effects of intravenous fluid viscosity on the accuracy of intravenous infusion flow regulators," *J. Korean Med. Sci.*, vol. 37, no. 9, 2022, doi: [10.3346/jkms.2022.37.e71](https://doi.org/10.3346/jkms.2022.37.e71).
- [9] O. Bacon and L. Hoffman, "System-level patient safety practices that aim to reduce medication errors associated with infusion pumps: An evidence review," *J. Patient Saf.*, vol. 16, no. 3, pp. S42–S47, Sep. 2020, doi: [10.1097/pts.0000000000000722](https://doi.org/10.1097/pts.0000000000000722).
- [10] E. S. Kirkendall, K. Timmons, H. Huth, K. Walsh, and K. Melton, "Human-based errors involving smart infusion pumps: A catalog of error types and prevention strategies," *Drug Saf.*, vol. 43, no. 11, pp. 1073–1087, Aug. 2020, doi: [10.1007/s40264-020-00986-5](https://doi.org/10.1007/s40264-020-00986-5).
- [11] S. Kuitunen, I. Niittynen, M. Airaksinen, and A.-R. Holmström, "Systemic causes of in-hospital intravenous medication errors: A systematic review," *J. Patient Saf.*, vol. 17, no. 8, pp. e1660–e1668, Dec. 2021, doi: [10.1097/pts.0000000000000632](https://doi.org/10.1097/pts.0000000000000632).
- [12] M. R. Islam, R. Z. Rusho, and S. M. R. Islam, "Design and implementation of low cost smart syringe pump for telemedicine and healthcare," in *Proc. IEEE Int. Conf. Robotics, Electrical Signal Process. Techn. (ICREST)*, Jan. 2019, pp. 440–444, doi: [10.1109/icrest.2019.8644373](https://doi.org/10.1109/icrest.2019.8644373).
- [13] M. Baeckert, M. Batliner, B. Grass, P. K. Buehler, M. S. Daners, M. Meboldt, and M. Weiss, "Performance of modern syringe infusion pump assemblies at low infusion rates in the perioperative setting," *Brit. J. Anaesthesia*, vol. 124, no. 2, pp. 173–182, Feb. 2020, doi: [10.1016/j.bja.2019.10.007](https://doi.org/10.1016/j.bja.2019.10.007).
- [14] G. Briganti and O. L. Moine, "Artificial intelligence in medicine: Today and tomorrow," *Frontiers Med.*, vol. 7, p. 27, Feb. 2020, doi: [10.3389/fmed.2020.00027](https://doi.org/10.3389/fmed.2020.00027).
- [15] S. Secinaro, D. Calandra, A. Secinaro, V. Muthurangu, and P. Biancone, "The role of artificial intelligence in healthcare: A structured literature review," *BMC Med. Informat. Decis. Making*, vol. 21, no. 1, p. 125, Apr. 2021, doi: [10.1186/s12911-021-01488-9](https://doi.org/10.1186/s12911-021-01488-9).
- [16] D. Lee and S. N. Yoon, "Application of artificial intelligence-based technologies in the healthcare industry: Opportunities and challenges," *Int. J. Environ. Res. Public Health*, vol. 18, no. 1, p. 271, Jan. 2021, doi: [10.3390/ijerph18010271](https://doi.org/10.3390/ijerph18010271).
- [17] L. Bai, "Chinese experts' consensus on the Internet of Things-aided diagnosis and treatment of coronavirus disease 2019 (COVID-19)," *Clin. eHealth*, vol. 3, pp. 7–15, Mar. 2020, doi: [10.1016/j.ceh.2020.03.001](https://doi.org/10.1016/j.ceh.2020.03.001).
- [18] M. R. Rosdi and A. Huong, "A smart infusion pump system for remote management and monitoring of intravenous (IV) drips," in *Proc. Comput. Appl. Ind. Electron. (ISCAIE)*, 2021, pp. 285–288, doi: [10.1109/ISCAIE51753.2021.9431790](https://doi.org/10.1109/ISCAIE51753.2021.9431790).
- [19] Z. Huang, Y. Li, T. Zhao, P. Ying, Y. Fan, and J. Li, "Infusion port level detection for intravenous infusion based on YOLO v3 neural network," *Math. Biosciences Eng.*, vol. 18, no. 4, pp. 3491–3501, 2021, doi: [10.3934/mbe.2021175](https://doi.org/10.3934/mbe.2021175).
- [20] N. Giaquinto, M. Scarpetta, M. A. Ragolia, and P. Pappalardi, "Real-time drip infusion monitoring through a computer vision system," in *Proc. Medical Meas. Appl., IEEE Int. Symp.*, 2020, pp. 1–5, doi: [10.1109/MeMeA49120.2020.9137359](https://doi.org/10.1109/MeMeA49120.2020.9137359).

- [21] N. Giaquinto, M. Scarpetta, M. Spadavecchia, and G. Andria, "Deep learning-based computer vision for real-time intravenous drip infusion monitoring," *IEEE Sensors J.*, vol. 21, no. 13, pp. 14148–14154, Jul. 2021, doi: [10.1109/JSEN.2020.3039009](https://doi.org/10.1109/JSEN.2020.3039009).
- [22] S. S. Agarwal, L. Kumar, K. H. Chavali, and S. C. Mestri, "Fatal venous air embolism following intravenous infusion," *J. Forensic Sci.*, vol. 54, no. 3, pp. 682–684, May 2009, doi: <https://doi.org/10.1111/j.1556-4029.2009.01004.x>.
- [23] M. W. Sowell, C. L. Lovelady, B. G. Brogdon, and C. H. Wecht, "Infant death due to air embolism from peripheral venous infusion," *J. Forensic Sci.*, vol. 52, no. 1, pp. 183–188, Jan. 2007, doi: [10.1111/j.1556-4029.2006.00307.x](https://doi.org/10.1111/j.1556-4029.2006.00307.x).
- [24] J. I. Westbrook, M. I. Rob, A. Woods, and D. Parry, "Errors in the administration of intravenous medications in hospital and the role of correct procedures and nurse experience," *BMJ Quality Saf.*, vol. 20, no. 12, pp. 1027–1034, Jun. 2011, doi: [10.1136/bmjqs-2011-000089](https://doi.org/10.1136/bmjqs-2011-000089).
- [25] A. Sutherland, M. Canobbio, J. Clarke, M. Randall, T. Skelland, and E. Weston, "Incidence and prevalence of intravenous medication errors in the U.K.: A systematic review," *Eur. J. Hospital Pharmacy*, vol. 27, no. 1, pp. 3–8, Oct. 2018, doi: [10.1136/ejpharm-2018-001624](https://doi.org/10.1136/ejpharm-2018-001624).
- [26] A. Karaca and Z. Durna, "Patient satisfaction with the quality of nursing care," *Nursing Open*, vol. 6, no. 2, pp. 535–545, Jan. 2019, doi: [10.1002/nop2.237](https://doi.org/10.1002/nop2.237).
- [27] S. H. Alsaqri, "Patient satisfaction with quality of nursing care at governmental hospitals, Ha'il city, Saudi Arabia," *J. Biol., Agricult. Healthcare*, vol. 6, no. 10, pp. 128–142, 2016.
- [28] M. L. Goh, E. N. K. Ang, Y.-H. Chan, H.-G. He, and K. Vehviläinen-Julkunen, "A descriptive quantitative study on multi-ethnic patient satisfaction with nursing care measured by the revised humane caring scale," *Appl. Nursing Res.*, vol. 31, pp. 126–131, Aug. 2016, doi: [10.1016/j.apnr.2016.02.002](https://doi.org/10.1016/j.apnr.2016.02.002).
- [29] J. Redmon, S. Divvala, R. Girshick, and A. Farhadi, "You only look once: Unified, real-time object detection," in *Proc. IEEE Conf. Comput. Vis. Pattern Recognit.*, Jun. 2016, pp. 779–788, doi: [10.1109/CVPR.2016.91](https://doi.org/10.1109/CVPR.2016.91).
- [30] J. Redmon and A. Farhadi, "YOLO9000: Better, faster, stronger," in *Proc. IEEE Conf. Comput. Vis. Pattern Recognit.*, Jul. 2017, pp. 6517–6525, doi: [10.1109/CVPR.2017.690](https://doi.org/10.1109/CVPR.2017.690).
- [31] K. M. Stacy. (2020). *Intravenous therapy: Dose and flow rate calculation-CE*. [Online]. Available: [http://repository.phb.ac.id/770/1/Intravenous-Therapy-Dose-and-Flow-Rate-Calculation-Skill\\_080520.pdf](http://repository.phb.ac.id/770/1/Intravenous-Therapy-Dose-and-Flow-Rate-Calculation-Skill_080520.pdf)
- [32] M. Hutton, "Numeracy skills for intravenous calculations," *Nursing Standard*, vol. 12, no. 43, pp. 49–56, Jul. 1998, doi: [10.7748/ns.12.43.49.s55](https://doi.org/10.7748/ns.12.43.49.s55).
- [33] A. Johnson and C. Brace, "Heat transfer within hydrodissection fluids: An analysis of thermal conduction and convection using liquid and gel materials," *Int. J. Hyperthermia*, vol. 31, no. 5, pp. 551–559, May 2015, doi: [10.3109/02656736.2015.1037799](https://doi.org/10.3109/02656736.2015.1037799).
- [34] D. Shubert, J. Leyba, and S. Niemann, *Chemistry and Physics for Nurse Anesthesia: A Student-Centered Approach*. Cham, Switzerland: Springer, 2017, pp. 214–216.
- [35] S. Spencer, H. Ipema, P. Hartke, C. Krueger, R. Rodriguez, A. E. Gross, and M. Gabay, "Intravenous push administration of antibiotics: Literature and considerations," *Hospital Pharmacy*, vol. 53, no. 3, pp. 157–169, Jun. 2018, doi: [10.1177/0018578718760257](https://doi.org/10.1177/0018578718760257).
- [36] F. Jamil, S. Ahmad, N. Iqbal, and D.-H. Kim, "Towards a remote monitoring of patient vital signs based on IoT-based blockchain integrity management platforms in smart hospitals," *Sensors*, vol. 20, no. 8, p. 2195, Apr. 2020, doi: [10.3390/s20082195](https://doi.org/10.3390/s20082195).
- [37] E. A. Mattox, "Complications of peripheral venous access devices: Prevention, detection, and recovery strategies," *Crit. Care Nurse*, vol. 37, no. 2, pp. e1–e14, Apr. 2017, doi: [10.4037/ccn2017657](https://doi.org/10.4037/ccn2017657).
- [38] International Council of Nurses. (Mar. 2021). *The Global Nursing Shortage and Nurse Retention*. ICN Policy Brief. [Online]. Available: <https://www.icn.ch/publications?year=2021&category=68>
- [39] Y. Kim, J. Seol, H. Lee, J. Lee, J. Park, and K. G. Kim, "Web-based intravenous fluid treatment monitoring platform in nursing station," *Surgical Innov.*, vol. 29, no. 5, pp. 677–680, Jan. 2022, doi: [10.1177/15533506211065849](https://doi.org/10.1177/15533506211065849).



**JAEHWANG SEOL** received the B.S. degree in biomedical engineering from Gachon University, Incheon, Republic of Korea, in 2023. From 2020 to 2023, he worked as an undergraduate researcher at the Medical Devices Research and Develop Center, Gachon University Gil Medical Center, Incheon. His research interests include robotics, control system modeling, deep learning for computer vision, and healthcare devices.



**SANGYUN LEE** received the M.S. degree in medical physics from Korea University, Seoul, South Korea, in 2019, and the Ph.D. degree from the Department of Health and Environmental Convergence Sciences, Korea University, in 2022. From 2016 to 2022, he was with Baekseok University, South Korea, where he had been engaged in the radiation safety management. From 2022 to 2023, he was with the Medical Devices Research and Development Center, Gachon University Gil Medical Center, South Korea, where he had been engaged in the Robotics and Optics Team. His research interests include AI fluorescence diagnosis surgery systems and medical physics.



**JEONGYUN PARK** received the B.S., M.S., and Ph.D. degrees in nursing from Seoul National University, Seoul, South Korea, in 1994, 2002, and 2015, respectively. Since 2010, she has been with the Department of Clinical Nursing, University of Ulsan, Ulsan, South Korea, where she is currently a Professor. Her research interests include oncology nursing, nutrition support, patient safety, and quality improvement in clinical settings.



**KWANG GI KIM** received the M.S. degree in physics from the Pohang University of Science and Technology, Pohang, South Korea, in 1998, and the Ph.D. degree in biomedical engineering from Seoul National University, Seoul, South Korea, in 2005. From 2007 to 2017, he was a Senior Researcher with the National Cancer Center, Goyang, South Korea. From 2017 to 2018, he was an Associate Professor with the Department of Biomedical Engineering, College of Health Science, Gachon University, Incheon, South Korea. Since 2018, he has been with the Department of Biomedical Engineering, College of Medicine and Health Science, with the Medical Devices Research and Development Center, Gachon University Gil Medical Center, and also with the Department of Health Sciences and Technology, Gachon Advanced Institute of Health Sciences and Technology (GAIHST), Incheon, Republic of Korea, where he is currently a Professor. His research interests include medical imaging process, medical robotics, and medical optics.

...